Kinetics of leucine-lysine peptide adsorption and desorption at –CH₃ and –COOH terminated alkylthiolate monolayers

Julia S. Apte
Department of Chemical Engineering, National ESCA and Surface Analysis Center for Biomedical Problems, University of Washington, Box 351750 Seattle, Washington 98195-1750

Lara J. Gamble
Department of Bioengineering, National ESCA and Surface Analysis Center for Biomedical Problems, University of Washington, Box 351750 Seattle, Washington 98195-1750

David G. Castner[a)]
Departments of Chemical Engineering and Department of Bioengineering, National ESCA and Surface Analysis Center for Biomedical Problems, University of Washington, Box 351750 Seattle, Washington 98195-1750

Charles T. Campbell[a)]
Department of Chemistry, University of Washington, Box 351700 Seattle, Washington 98195-1700

The kinetics of adsorption and desorption of two highly asymmetrical model peptides were studied at methyl- and carboxylic acid-terminated alkylthiolate self-assembled monolayer (SAM) surfaces on gold. The model peptides were leucine-lysine (LK), α-helical (LKα14), and β-strand (LKβ15) peptides that have a well-defined secondary structure with the leucines localized on one side and the lysines on the other side. These secondary structures were previously shown to be maintained after adsorption and to control LK peptide orientation on these surfaces. The kinetics of peptide adsorption were analyzed by surface plasmon resonance as a function of peptide solution concentrations at pH 7.4. Peptide desorption was measured by rinsing with a buffer at various times along the adsorption curve. Both peptides had a saturation coverage of approximately 1 ML (monolayer) on the carboxyl SAM. Both peptides exhibited mostly irreversible binding on both surfaces, but the LKα14 peptide showed some limited reversible binding. Reversibly bound peptides could be in the second adlayer interacting only with peptides in the first layer or peptides interacting with a partially covered adsorption site and therefore not able to fully bind to the SAM surface. The near complete lack of reversible binding for LKβ15 is possibly due to strong peptide-peptide hydrogen bonding in β-sheet structures within the adsorbed layer. For a given dose of either peptide, much less peptide adsorbed on the methyl SAMs. The adsorption rate of irreversibly bound LKα14 on carboxylic acid SAMs was first-order with respect to solution concentration. Both peptides showed nucleation-like adsorption kinetics on the carboxylic acid SAM, indicating that peptide-peptide bonding is needed to stabilize the adsorbed layer. Adsorption on the methyl SAM was much lower in quantity for both peptides and seemed to require prior aggregation of the proteins in solution, at least for LKβ15. © *2010 American Vacuum Society.* [DOI: 10.1116/1.3494080]

I. INTRODUCTION

Understanding biological interactions with surfaces provides important information for the design of engineered biomaterials. The interactions of proteins with implantable or diagnostic biomaterials decide whether or not it will serve the purpose for which it was designed.[1,2] A diagnostic chip cannot be used if it is a subject to false positives from non-specific protein fouling.[3–5] An implanted glucose sensor cannot function if it has been walled off via fibrous encapsulation from the blood stream.[6] Proteins, however, are very complex, as are usually the surfaces to which they are adhering, and so interpreting these protein-surface interactions can be challenging.

Peptides provide a model system for investigating protein interactions because they reduce the complexity of the system. Leucine-lysine (LK) peptides[7] with well-defined secondary structures have been used previously to study peptide interactions with well-defined surfaces.[8–18] Our previous work examined the adsorption of two model LK peptides, an α-helical (LKα14) and a β-strand (LKβ15) peptide, onto methyl- and carboxylic acid-terminated alkylthiol self-assembled monolayers (SAMs) using x-ray photoelectron spectroscopy (XPS), time-of-flight secondary ion mass spectrometry, sum-frequency generation vibrational spectroscopy, and near-edge x-ray absorption fine structure spectroscopy.[10,14] The α-helix peptide is a 14-mer, and the β-strand is a 15-mer, of hydrophilic lysine and hydrophobic

---
a)Authors to whom correspondence should be addressed; electronic addresses: castner@nb.uw.edu and campbell@chem.washington.edu

leucine residues with hydrophobic periodicities of 3.5 and 2, respectively. These periodicities result in the formation of the peptides' secondary structure since they will fold such that the leucine side chains are located on one side of the peptides and the lysine side chains on the other side. Previous results showed that the secondary structures in both peptides are preserved upon adsorption.[8–18] The peptide backbones are aligned nominally parallel to the SAM surfaces with the lysine side chains oriented toward the carboxylic acid SAM surface and the leucine side chains oriented toward the methyl SAM surface. Thus, these peptide lysine side chains seem to be electrostatically bonded to the –COOH surface while the leucine side chains seem to be bonded to the methyl surface via hydrophobic interactions. Note that the –COOH surface is thought to be about 50% deprotonated at *p*H 7.4, which was the *p*H condition for those studies as well as the work presented here.[19]

This article further explores these very well-defined peptide-SAM interactions by studying their adsorption and desorption kinetics using surface plasmon resonance spectroscopy (SPR). The results help define the rate laws and rate constants for their adsorption and desorption and show that strong peptide-peptide bonding is necessary to stabilize these peptide adlayers and/or facilitate their adsorption.

SPR is a technique that detects changes in refractive index near a gold surface. By flowing a solution containing the molecule of interest over the sensor surface, the amount of surface binding can be determined by the shift in the plasmon resonance conditions.[20] This shift can be quantitatively converted to a change in refractive index, and finally to the mass per unit area or effective depth of the surface adsorbate.[21] Because the measurement can be done in real time (with ~1 s resolution), it can be used to measure the adsorption (k_a) and desorption (k_d) rates. This technique has been used previously to investigate a wide range of biomolecule-surface interactions, including fouling of surfaces, biomarker specificity, and probe-target interactions.[22–26]

II. MATERIALS AND METHODS

A. SAM preparation

SPR low-fluorescence BK7 glass slides (Schott Glass Technology) were coated with a thin 2 nm adhesion layer of Cr followed by a 50 nm layer of Au (99.99%) by electron beam evaporation at pressures below 1×10^{-6} Torr. The self-assembled monolayers used in this study were dodecane thiol and 11-mercapto-undecanoic acid thiol (Aldrich). SAMs were prepared *ex situ* in 1 and 0.5 mM ethanolic solutions, respectively. They were allowed to assemble for approximately 24 h at room temperature under a nitrogen atmosphere. The dodecane SAMs were then rinsed copiously with ethanol to remove any unbound or oxidized sulfur compounds. The undecanoic acid SAMs were placed in 50 ml vials of ethanol, mixed by a vortex three times for approximately 10 s, and then rinsed thoroughly with ethanol. Both

were then dried under a stream of nitrogen and stored under a nitrogen atmosphere.

B. Peptide synthesis

Amino acids used in this study were Fmoc-Leu-OH and Fmoc-Lys(Boc)-OH (Novabiochem). The peptides were synthesized on a PS3 solid-state peptide synthesizer (Rainin) on a Leu-Wang resin (Novabiochem). O-(benzotriazole-N,N,N',N'-tetramethyluronium hexafluorophosphate (HBTU) (Advanced ChemTech) was used as an activator, and the *N*-termini of the resin-bound peptides were capped following synthesis by acetylation with about 3 ml of acetic anhydride. Peptides were cleaved from the resin, dried by overnight lyophilization and their purity was checked using mass spectrometry following the procedures outlined by Long *et al.*[9] The final peptide sequences were Ac-LKKLLKLLKKLLKL-OH for LKα14 and Ac-LKLKLKLKLKLKLKL-OH for LKβ15.

C. Solutions

Phosphate buffered saline (PBS) 10× solution from Omnipur (EMD) was diluted fivefold with de-ionized water to make 2× PBS solutions that were degassed before use. Peptide solutions were all made in degassed, de-ionized water and then mixed with equal volumes of degassed 2× PBS to make solutions in 1× PBS (137 mM NaCl, 3 mM KCl, 10 mM phosphate salts for 1× solution, *p*H ~ 7.4). It was found that this method reduced peptide aggregation. Also, equal parts of degassed water and 2× PBS were mixed to make the 1× PBS used for initial stabilization of the system and for rinsing. Below, we refer to 1× PBS solutions as simply "PBS."

D. SPR

Measurements were done using a four-channel SPR system (Institute of Photonics and Electronics, Prague, Czech Republic),[27–29] that is set up in the Kretschmann configuration. It measures the wavelength shift in the dip of reflected light at a fixed angle. The solutions were flowed through a flow cell at 70 μl/min. One channel was always used as a reference channel to detect fluctuations in ambient conditions and instrument drift. The signal from this reference channel was subtracted from the signals of the other channels.

Quantification of peptide adsorption was done using the method outlined by Campbell and Kim,[20] using Eq. (1).

$$d_{\text{eff}} = \lambda \left[\frac{\Delta R}{S(\eta_a - \eta_s)} \right], \tag{1}$$

where d_{eff} is the effective depth of adsorbate on the surface, λ is a parameter (SPR probe depth) that is 129 nm for these conditions, ΔR is the measured wavelength shift in nm, S is this SPR instrument's sensitivity (2800 nm per refractive index unit, determined using mixtures of ethylene glycol and water), η_a is the refractive index of the adsorbing peptide, and η_s is the index of refraction of the PBS/peptide solution used here, which was measured to be 1.3354 ± 0.0001. The

surface coverage of the peptide (in grams per unit area) is obtained from d_{eff} by simply dividing by the peptide's specific volume.[20]

Both η_a and the peptides' specific volume were assumed to be the same as those for most proteins, 1.57 and 0.77 cm³/g, as noted by Jung *et al.*[21]

III. RESULTS AND DISCUSSION

The adsorption kinetics of these peptides onto the freshly prepared SAMs were measured by SPR at room temperature. This was done by first introducing pure PBS into the flow cell containing the fresh SAM, and then switching from PBS solution to a solution containing the peptide while monitoring the SPR signal (adsorbed amount) versus time. This switch from pure PBS to peptide in PBS was initially done at flow rates of 50, 70, and 90 μl/min, and it was found that values greater than 50 μl/min were required to avoid the mass-transport-limited regime. For this reason, all experiments reported below were done at a flow rate of 70 μl/min. After adsorption, the desorption kinetics were studied by using SPR to monitor the amount of adsorbed peptide versus the rinsing time after switching back to pure PBS at the same flow rate. Adsorption and desorption kinetics were, thus, measured for both LKα14 and LKβ15 at 0.1 and 0.01 mg/ml peptide solution concentrations on both the –COOH and methyl surfaces. Typical results are shown in Fig. 1. No significant adsorption of either peptide was observed at 0.01 mg/ml on the methyl surface (not shown). This is consistent with our recent results, which showed that much higher concentrations of these peptides were required to obtain monolayer coverage on the methyl SAM surfaces compared to the –COOH SAM surfaces.[10,14]

To determine if the reversibility of peptide adsorption was a function of the time it had spent on the surface, a PBS buffer was reintroduced into the flow cell at different time points along these SPR adsorption curves. The amount removed after 5 min of rinsing was used as a measure of the reversibly adsorbed amount, and this was subtracted from the total amount adsorbed (as measured by SPR just before rinsing) to give the irreversibly adsorbed amount.

Figure 2 shows a compilation of the irreversibly and reversibly bound peptide surface concentrations as a function of peptide dose (concentration × time) for two solution concentrations of LKα14 adsorption onto the carboxylic acid SAMs. This is the case that exhibits the largest amount of reversibly bound peptide, but even here it is only ~20 ng/cm², compared to ~140 ng/cm² for the total amount of peptide adsorption at saturation coverage. As seen, the fractional amounts of the reversible and irreversible bound LKα14 peptides grow at similar rates with that of the peptide dose, with both saturating by about 0.1 mg ml⁻¹ min. Its low signal compared to the scatter prevents any more quantitative analysis of the rate of buildup of the small reversibly bound LKα14 peptide.

Similar data to Fig. 2 for the other peptide/surface combinations showed that the amount of reversibly bound peptide was only ~3 ng/cm² for LKβ15 on carboxylic acid
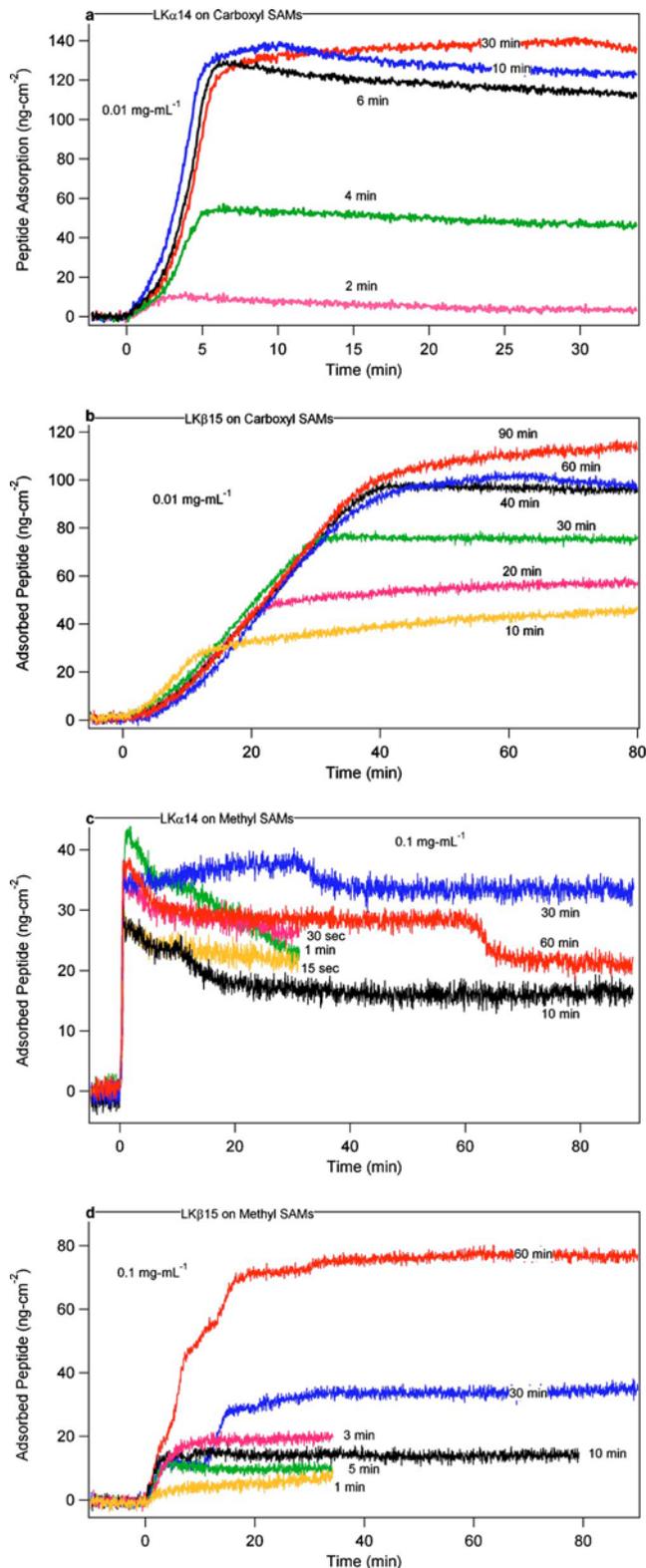
FIG. 1. (Color online) Adsorbed amount (by SPR) vs time during adsorption/intermittent-rinsing experiments for (a) LKα14 and (b) LKβ15 onto carboxylic acid SAMs, and (c) LKα14 and (d) LKβ15 onto methyl SAMs. Before time 0, only PBS was flowing across the clean surface. Peptide was introduced starting at time 0 in a 0.01 or 0.1 mg/ml PBS solution, then the surface was rinsed with PBS at the times indicated. As can be seen, very little peptide is removed upon rinsing, and thus these peptides' adsorption is dominantly irreversible on both surfaces, but LKα14 shows more reversible binding than LKβ15.
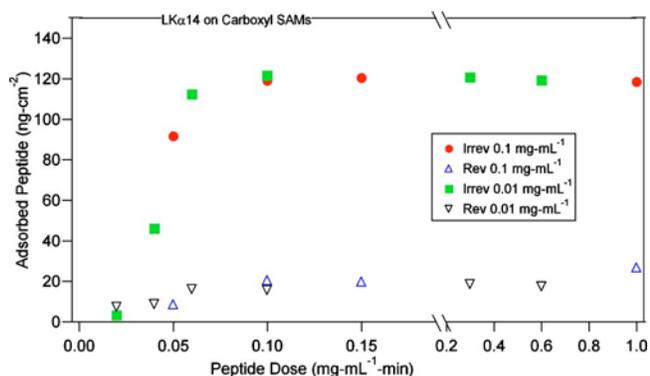
FIG. 2. (Color online) Irreversibly and reversibly bound peptide amounts as a function of peptide dose for LKα14 adsorption onto carboxylic acid SAMs. Dose is the solution concentration multiplied by the time of exposure.

SAMs, ~6 ng/cm^2 for LKα14 on methyl SAMs, and <2 ng/cm^2 for LKβ15 onto methyl SAMs. In these cases, the reversibly adsorbed amounts are so small that the total peptide adsorption amounts versus time, measured by the SPR curves in Figs. 1(b)–1(d) for these systems, essentially reflect the kinetics of their irreversible adsorption. The amount of reversibly bound peptide was so small compared to the scatter in these cases that no conclusions can be drawn concerning their rate of formation.

The LKα14 peptide showed more reversible binding on both surfaces than the LKβ15 peptide. Reversibly bound peptides could be in the second adlayer interacting only with peptides in the first layer, or peptides interacting with a partially covered adsorption site and, therefore, not able to fully bind to the SAM surface. The near complete lack of reversible binding for LKβ15 is possibly due to strong peptide-peptide hydrogen bonding in β-sheet structures within the adsorbed layer, which prevents its desorption.

As seen above, LKα14 adsorption onto to the methyl SAMs was mostly irreversible, probably due to hydrophobic interactions between its leucine methyl groups and the methyl groups of the SAMs, as suggested by the leucine-down structure we reported previously for this peptide on the methyl SAM surface.[10,14] This structure means the leucine groups of the irreversibly adsorbed peptide would not be available for binding a second layer of peptides through leucine-leucine hydrophobic interactions. Therefore, the small amount of reversibly bound peptide observed on this surface must come from peptides loosely bound to the SAM surface. Previous XPS results show the amount of LKα14 peptide irreversibly bound from a 0.1 mg/ml solution was less than 1 ML (monolayer) on the methyl SAMs and more than 1 ML on the carboxyl SAMs.[10] This is consistent with the SPR results that show approximately 40 ng/cm^2 of peptide adsorption onto the methyl SAM compared to 150 ng/cm^2 of peptide adsorption onto the carboxyl SAM. A close-packed monolayer of LKα14 on the surface was estimated to be around 90 ng/cm^2. (Here, the bulk density was used to estimate packing density assuming that the pep-

tides pack with their long axis along the surface, and using the dimensions calculated by molecular simulations.)[10]

As noted above, the reversibly adsorbed amounts in Fig. 1(b)–1(d) are so small that the total peptide adsorption amounts versus time, as measured by these SPR curves, essentially reflect the kinetics of their irreversible adsorption. Also, Fig. 2 showed that the growth of the reversibly and irreversibly adsorbed amounts in Fig. 1(a) follow very similar rates (fraction of saturation amount versus time), and the reversible amount was only ~14% of the total SPR signal. Thus, the kinetics reflected by the SPR curves in all four parts of Fig. 1 essentially reflect both the total adsorbed amounts and the irreversibly adsorbed amounts versus time. We will describe these kinetics next.

From inspecting these SPR curves, it is clear that both (a) LKα14 and (b) LKβ15 adsorptions onto carboxylic acid SAMs show rates that initially accelerate with time (or adsorbed amount), and then rather abruptly saturates at approximately the amount expected for a close-packed monolayer. As we will explain in more detail below, this acceleration in adsorption rate with time, or apparent induction period, indicates a nucleation phenomenon whereby the binding of an isolated peptide alone to the surface is not sufficiently strong to remain there, unless it is joined by one or more other peptides to nucleate a cluster or a small two-dimensional (2D) island of adsorbed peptides, which mutually stabilize each other through peptide-peptide bonding. The weakly held, isolated peptides, though only transiently adsorbed on the –COOH SAMS, serve as precursors to the more strongly bound peptides in the 2D islands. This induction period is also obvious in Fig. 2.

For LKα14 adsorbing onto methyl SAMs [Fig. 1(c)], there is no such induction period. Adsorption occurs rapidly from the start, but it stops growing at a very low coverage (only ~1/3 of a close-packed monolayer). Thereafter, the amount of peptide rather surprisingly decreases by ~20% with an increasing dose for most runs. This may be related to some of the peptides changing geometry with time, and in doing so destabilizing other peptides. Our previous results[10,14] showed that the leucine side of this peptide is oriented toward the methyl SAM surface in the final structure, so that it can bond to the methyl surface via hydrophobic interactions. This prevents strong hydrophobic peptide-peptide interactions stabilizing peptides in the second layer. Perhaps some peptides initially adsorb in a different structure that allows enough peptide-peptide interactions to keep other peptides on the surface near them, but this possibility goes away when the peptide eventually reaches its most stable structure. It is difficult to understand why the saturation coverage is so low relative to a close-packed monolayer. Because the peptides are oriented on the surface and thus each one has a dipole moment pointing normal to the surface in the same direction, peptide-peptide interactions are expected to be repulsive due to dipole-dipole repulsions. This may prevent higher packing densities on the surface.

The adsorption kinetics of LKβ15 onto methyl SAMs [Fig. 1(d)] is even more complex. Here, adsorption seems to

proceed in an erratic, stepwise fashion where periods of apparent saturation are followed by periods of rapid adsorption, as if there are several, steplike induction periods. We postulate that this may be due to inhomogeneities in the extent of peptide aggregation in the flow cell. These data were taken at the highest peptide concentration achievable without visible evidence of aggregation (0.1 mg/ml). Even here there are probably small clusters in the solution. These may be the only peptides that can adsorb. These peptide-peptide attractions may be essential for stabilizing the adsorbed layer. This is similar to the nucleation effect needed to explain Figs. 1(a) and 1(b), but here it may be nucleation in the solution phase rather than on the surface that makes adsorption possible. The complete lack of protein adsorption observed at tenfold lower concentration is consistent with such a model. The uptake was also very irreproducible after the first steplike uptake of ~15 ng/cm^2 [for example, compare the first 30 min of the top 2 curves in Fig. 1(d)], which is also understandable in such a model. It is not clear why there would be inhomogeneities in the extent of peptide aggregation at different places in the flowing stream of solution, but since aggregation is a highly nonlinear phenomenon, it may be possible.

A. LKα14 adsorption and desorption kinetics on carboxylic acid SAMs

Since there are two types of interactions between this LK peptide and this –COOH SAM surface, irreversible and reversible binding, the peptide adsorption kinetics were modeled using a two-site model. First, to determine whether the concentration dependence was due to kinetic-limited or mass-transport-limited rates, the half-times of adsorption were determined for LKα14 adsorbing onto the carboxyl SAMs at various peptide solution concentrations. At each concentration, we determined the half-time of irreversible adsorption ($t_{1/2,I}$), i.e., the time it takes to reach half of the maximum amount of irreversibly bound peptide, from the data in Fig. 2 and similar data for other concentrations. The common logarithm of these times was plotted versus the common logarithm of the peptide solution concentration (Fig. 3) and it was found that the relationship was first-order (slope=1), meaning that the adsorption kinetics observed were rate-limited rather than mass-transport-limited (a second order process).[23] There was a concentration limit above which the linearity of the curve broke down, probably because the half-life of these high concentrations approaches the response time of the instrument. This instrument response time was estimated by measuring the half-time required for the SPR signal to respond to the refractive index change associated with simply changing from one calibration solution to another (different concentrations of ethylene glycol in water), and found to be ~0.7 min. This limit, represented by a dashed line in Fig. 3, is due to the design of the fluidics system.

The first-order dependence of LKα14 adsorption is further confirmed by the data in Fig. 4. Here, the adsorption curves at different peptide solution concentrations have been
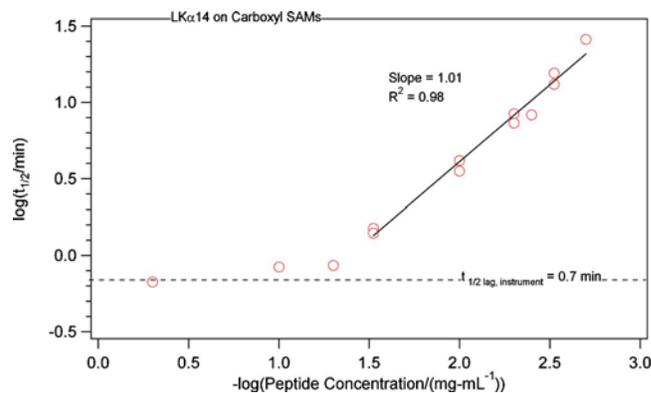
FIG. 3. (Color online) Plot showing the $\log_{10}$ of the half-time of irreversible adsorption vs the $\log_{10}$ of peptide concentration for LKα14 adsorption onto carboxylic acid SAMs. The slope of 1.01 indicates that the concentration dependence of the adsorption rate is first-order.

plotted as a function of dose. In such a plot, if the adsorption were first-order with respect to concentration, the curves would collapse onto each other. This is essentially the case for the lower concentrations, but not at the two higher concentrations (0.1 and 0.5 mg/ml). At the higher concentrations, the adsorption is slower due to the slower instrument response time.

Adsorption curves from Fig. 4 for concentrations within the linear regime of Fig. 3 were fitted using a double-exponential model [Eqs. (2)–(5)][30–34] to describe the sum of the irreversible and reversible adsorption curves (each assumed to be first-order Langmuir adsorption kinetics).

The double-exponential model is given by

$$\Delta R = R_{\infty,\text{irrev}}(1 - e^{-k_{\text{irrev}}t}) + R_{\infty,\text{rev}}(1 - e^{-k_{\text{rev}}t}), \qquad (2)$$

where
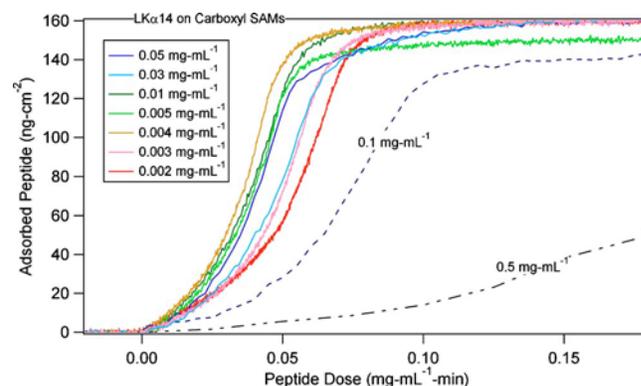
FIG. 4. (Color online) SPR curves of LKα14 peptide adsorption amount onto carboxyl SAMs vs dose (constructed from the SPR signal vs time curves) at different peptide concentrations for LKα14 on carboxylic acid SAMs. The close overlap of the curves at low concentrations confirms that the rate is nearly first-order in solution concentration of the peptide, but this breaks down at the higher concentrations due to the slow time response of the instrument. At all solution concentrations, a significant increase in slope (rate) with dose was observed during the initial stages of adsorption, indicating that adsorption gets faster with increasing peptide surface coverage at first. This suggests some nucleation-type kinetic effect during the initial binding events. Eventually the surface saturates at ~150±10 ng/cm^2.
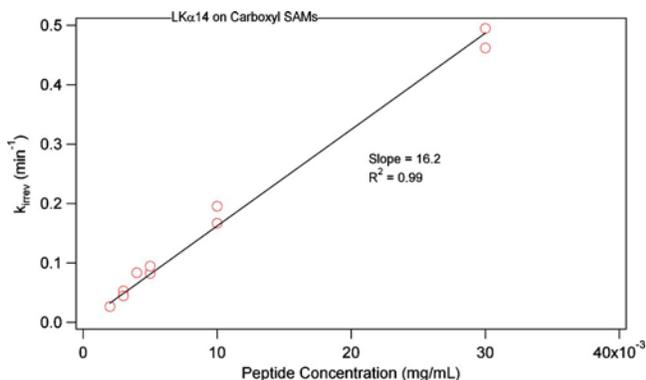
FIG. 5. (Color online) Graph showing k_{irrev} (equal to $\ln 2 / t_{1/2,I}$) vs peptide concentration for LKα14 on carboxylic acid SAMs. As seen in Eq. (3), the line fit to these data gives $k_{a,I}$ from the slope. Thus, $k_{a,I}$ was found to be 16.2 ml mg^{-1} min^{-1}.

$$k_{\mathrm{irrev}} = \frac{\ln 2}{t_{1/2,I}} = (k_{a,I}[C]), \qquad (3)$$

$$k_{\mathrm{rev}} = \frac{\ln 2}{t_{1/2,R}} = (k_{a,R}[C] + k_{d,R}). \qquad (4)$$

Given Eqs. (3) and (4), Eq. (2) can also be written as

$$\Delta R = R_{\infty,\mathrm{irrev}}(1 - 2^{-t/t_{1/2,I}}) + R_{\infty,\mathrm{rev}}(1 - 2^{-t/t_{1/2,R}}), \qquad (5)$$

where ΔR is the total SPR response, $R_{\infty,\mathrm{irrev}}$ is the equilibrium response for the irreversible portion of the curve at that concentration, $R_{\infty,\mathrm{rev}}$ is the equilibrium response for the reversible part of the curve, and k_{irrev} and k_{rev} are the observed pseudo-first-order rate constants.

Although the irreversible adsorption is first-order with respect to concentration, the adsorption curves do not exactly follow the exponential shape of a Langmuir adsorption curve, as there is a significant acceleration in adsorption rate during the first part of the adsorption curves, as seen in Figs. 2 and 4. Therefore, fitting the curves to the exponential
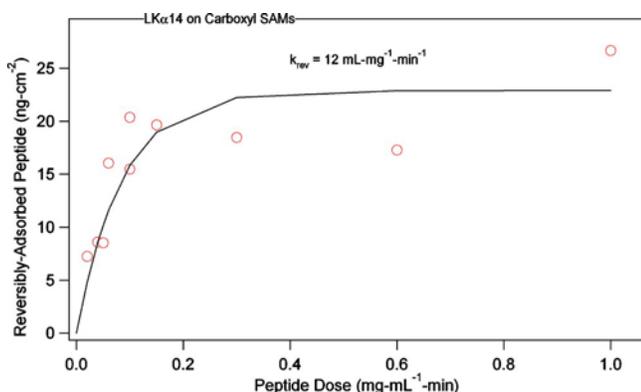
FIG. 6. (Color online) Reversibly bound peptide surface concentration as a function of peptide dose (concentration times exposure time) for LKα14 on carboxylic acid SAMs. These data were fitted to a single exponential model and k_{rev} was found to be approximately 12 ml mg^{-1} min^{-1}. Due to the variability in the reversibly bound peptide data, the kinetic constants only provide an order of magnitude estimate of k_{rev}.
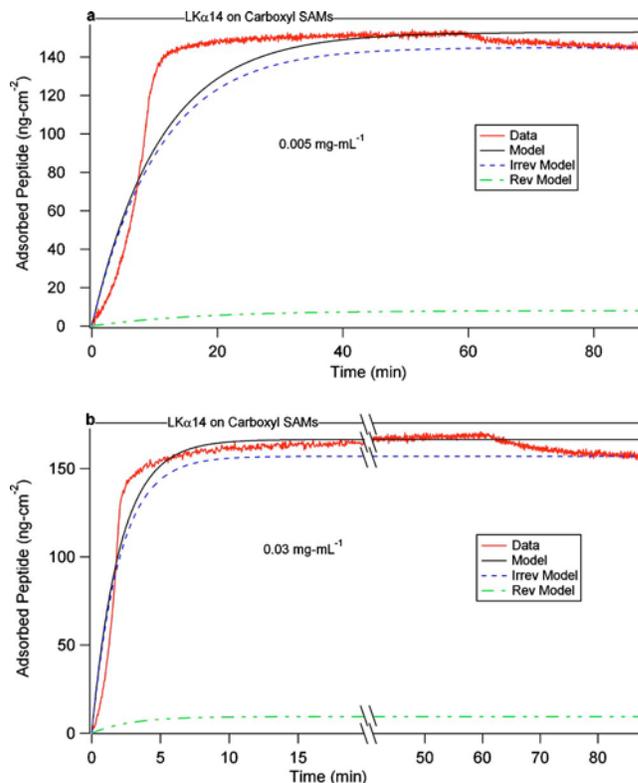
FIG. 7. (Color online) Adsorption amount vs time and kinetic models for LKα14 adsorption onto carboxylic acid SAMs from PBS solution with peptide concentrations of (a) 0.005 mg/ml and (b) 0.03 mg/ml. At the lower solution concentrations, there is a significant acceleration in adsorption rate in the first 10 min, leading to a noticeable disagreement between the model and experimental data in this region. However, this two-exponential model was able to reproduce the average rate of adsorption (half-life) at different concentrations, as also shown by the linear k_{irrev} dependence on concentration [Fig. 4]. [Note the split axis in (b).]

model of Eq. (2) using least-squares regression was not possible. Instead, the $t_{1/2,I}$ values from Fig. 3 [converted to k_{irrev} values using Eq. (3)] were plotted versus their peptide solution concentration (Fig. 5) to yield the first-order adsorption rate constant for irreversible binding, $k_{a,I}$, of 16 ml/mg min.

The reversible adsorption, however, did seem to follow an exponential curve and there was no initial acceleration in adsorption as with the irreversible adsorption [Fig. 2]. Therefore, it was possible to fit the reversible data of Fig. 2 to the reversible portion of the exponential model of Eq. (2) using least-squares regression (Fig. 6), and it was found that $k_{\mathrm{rev}}/[C]$ is on the order of 12 ml/mg min. Because of the scatter in the reversible adsorbed amount ($R^2 = 0.68$), this can only be taken as an order of magnitude estimate for k_{rev}.

Using these values found for k_{irrev} and k_{rev}, adsorption data of two concentrations were fitted to this two-exponential model. Figure 7 shows two sets of data at different concentrations within the linear regime of Fig. 3 (0.005 and 0.03 mg/ml LKα14) and their double-exponential models using the calculated $t_{1/2,I}$ and k_{rev}, for comparison. Because the first-order exponential curves cannot accommodate the initially increasing slope of the irreversible adsorption curve, the model does not exactly describe the data, especially at
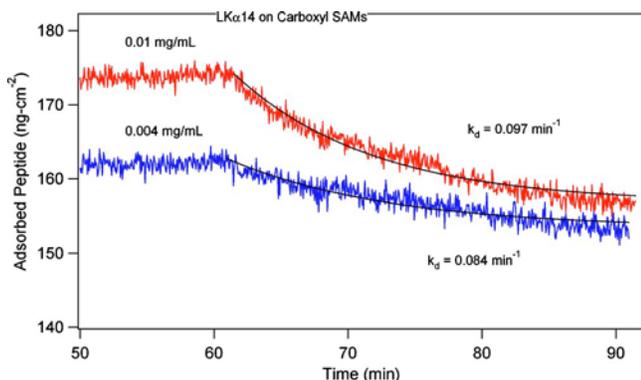
FIG. 8. (Color online) Exponential decay models describing peptide desorption for LKα14 on carboxylic acid SAMs. Slightly faster desorption was often seen for the adsorption curves from higher solution concentrations, indicating the presence of more weakly bound peptides on the surface. (The data are not offset.)

the lower peptide solution concentrations [Fig. 7(a)]. The initially increasing slope strongly suggests the dominance of some nucleation event required before further adsorption can proceed, probably associated with the slow nucleation of small 2D islands of the adsorbed peptide on the surface before further adsorption can proceed rapidly. This is not captured by simple first-order Langmuir adsorption kinetics, and again highlights the importance of peptide-peptide interactions in this system's adsorption/desorption properties. However, this double-exponential model does capture the average adsorption rate (half-life) of this peptide versus concentration. At higher peptide solution concentrations [Fig. 7(b)], this nucleation effect may still be present but becomes less obvious due to the limitations of the instrument response time.

At first, it would seem that the first-order dependence in the adsorption rate would be inconsistent with the proposed nucleation kinetics, since the formation of nuclei requires several peptide molecules. However, if the density of nuclei (number per unit area) is small and independent of concentration, this is expected. The density of adsorbate nuclei is independent of concentration whenever they form at surface defects, which are present on the starting surface in a fixed number density (the so-called heterogeneous nucleation); this contrasts with homogeneous nucleation where clusters form on perfect parts of the surface, such that their density is a function of solution concentration (although often only a very weak function even there).[35]

Finally, the desorption curves were modeled to determine the dissociation rate constant. It was observed that, typically after adsorption from lower concentrations, there was a very gradual desorption. After dosing higher adsorption concentrations, there was a slightly more rapid desorption process. However, there was quite a bit of variability in the reversible data. Two representative curves were fitted to obtain approximations of the desorption constant (Fig. 8). The curves after dosing at 0.004 and 0.01 mg/ml were fitted to the first-order Langmuir desorption rate equation[32,33]

$$\Delta R = R_{\infty,\text{irrev}} + R_{\infty,\text{rev}}(e^{-k_d(t-t_{\text{rinse}})}), \qquad (6)$$

where k_d is the desorption rate and t_{rinse} is the time at which the buffer was introduced into the flow cell. The resulting values of k_d were 0.08 min^{-1} ($R^2 = 0.83$) for 0.004 mg/ml and k_d of 0.1 min^{-1} ($R^2 = 0.94$) for 0.01 mg/ml. As stated, because of the high degree of variability in the reversible data, these values should only be interpreted as an order of magnitude estimate for the dissociation rate constants. The desorption models of Eq. (6) and Fig. 8 describe the desorption data well, and it can be hypothesized that the slightly faster desorption process may represent more weakly bound peptides, either from a second layer of peptides or from peptides that cannot fully bind to the SAM surface. This is consistent with the fact that faster desorption rates were more often seen from adsorption at higher solution concentrations where a second layer of peptides would be more likely to form.

IV. CONCLUSIONS

Peptide adsorption behavior was studied for an α-helical (LKα14) and a β-strand (LKβ15) peptide on methyl and carboxylic acid SAM surfaces. The reversibility of adsorption at different time points along the adsorption curve was monitored using an intermittent-rinsing technique, where PBS buffer was reintroduced into the flow cell at different time points. These data showed that both peptides had a saturation coverage of approximately 1 close-packed monolayer on the carboxyl SAMs. Adsorption of the LKα14 peptide onto carboxylic acid SAMs was mainly irreversible, with a small amount of reversibly bound peptide. This reversibly bound layer might be a second layer whose leucine side chains are interacting with the leucines of the irreversibly bound layer, or peptides that can only partially interact with the SAM surface due to steric crowding. Both peptides showed much lower adsorption amounts onto the methyl SAMs for the same solution concentration, as observed in previous XPS studies, and saturation coverage far below a close-packed monolayer. This is indicative of the weaker interactions of the peptides with (most of) the methyl SAM surface. LKα14 adsorption onto the methyl surface was mostly irreversible with some reversible binding. LKβ15 on the carboxyl and methyl surfaces showed almost exclusively irreversible binding, most likely due to the interpeptide hydrogen bonding in the β-sheet structures that likely stabilized those peptides on the surface. Kinetic analysis for LKα14 adsorbing onto the carboxyl surface showed that the adsorption rate of the peptides was first-order with respect to peptide solution concentration, but not first-order in the free site concentration. A first-order Langmuir model (that allowed separate rate constants for reversible and irreversible adsorption) deviated strongly from the SPR data in the early part of the adsorption curve, such that an induction period was observed initially, wherein the rate of adsorption grew with an increasing coverage. This suggests that a nucleation of clusters of adsorbed peptides is initially required for further adsorption. The desorption behavior displayed variability de-

pending on the amount of reversibly bound peptide on the surface, but fitting an exponential model to representative curves gave an order of magnitude estimate for the desorption constant of 0.1 min^{-1} for the reversibly bound peptides. Adsorption of LKβ15 onto the methyl SAM seemed to require peptide aggregation in solution prior to adsorption to achieve a coverage above ~15 ng/cm^2.

ACKNOWLEDGMENTS

[1] D. G. Castner and B. D. Ratner, Surf. Sci. **500**, 28 (2002).
[2] *Proteins at Interfaces II: Fundamentals and Applications*, edited by T. A. Horbett and J. L. Brash (American Chemical Society, Washington, 1995), Vol. 602, p. 1.
[3] H. Vaisocherová, Z. Zhang, W. Yang, Z. Q. Cao, G. Cheng, A. D. Taylor, M. Piliarik, J. Homola, and S. Y. Jiang, Biosens. Bioelectron. **24**, 1924 (2009).
[4] M. Ebara, J. M. Hoffman, P. S. Stayton, and A. S. Hoffman, Radiat. Phys. Chem. **76**, 1409 (2007).
[5] P. Wu, D. G. Castner, and D. W. Grainger, J. Biomater. Sci., Polym. Ed. **19**, 725 (2008).
[6] M. C. Frost *et al.*, Microchem. J. **74**, 277 (2003).
[7] W. F. DeGrado and J. D. Lear, J. Am. Chem. Soc. **107**, 7684 (1985).
[8] N. T. Samuel, Ph.D. thesis, University of Washington, 2005.
[9] J. R. Long, N. Oyler, G. P. Drobny, and P. S. Stayton, J. Am. Chem. Soc. **124**, 6297 (2002).
[10] J. S. Apte, G. Collier, R. A. Latour, L. J. Gamble, and D. G. Castner, Langmuir **26**, 3423 (2010).
[11] N. F. Breen, T. Weidner, K. Li, D. G. Castner, and G. P. Drobny, J. Am. Chem. Soc. **131**, 14148 (2009).
[12] O. Mermut, D. C. Phillips, R. L. York, K. R. McCrea, R. S. Ward, and G. A. Somorjai, J. Am. Chem. Soc. **128**, 3598 (2006).
[13] D. C. Phillips, R. L. York, O. Mermut, K. R. McCrea, R. S. Ward, and G. A. Somorjai, J. Phys. Chem. C **111**, 255 (2007).
[14] T. Weidner, J. S. Apte, L. J. Gamble, and D. G. Castner, Langmuir **26**, 3433 (2010).
[15] T. Weidner, N. F. Breen, G. P. Dobny, and D. G. Castner, J. Phys. Chem. B **113**, 15423 (2009).
[16] T. Weidner, N. T. Samuel, K. McCrea, L. J. Gamble, R. S. Ward, and D. G. Castner, BioInterphases **5**, 9 (2010).
[17] R. L. York, W. K. Brown, P. L. Geissler, and G. A. Somorjai, Isr. J. Chem. **47**, 51 (2007).
[18] R. L. York, O. Mermut, D. C. Phillips, K. R. McCrea, R. S. Ward, and G. A. Somorjai, J. Phys. Chem. C **111**, 8866 (2007).
[19] K. P. Fears, S. E. Creager, and R. A. Latour, Langmuir **24**, 837 (2008).
[20] C. T. Campbell and G. Kim, Biomaterials **28**, 2380 (2007).
[21] L. S. Jung, C. T. Campbell, T. M. Chinowsky, M. N. Mar, and S. S. Yee, Langmuir **14**, 5636 (1998).
[22] C. Y. Lee, L. J. Gamble, D. W. Grainger, and D. G. Castner, BioInterphases **1**, 82 (2006).
[23] L. S. Jung, K. E. Nelson, P. S. Stayton, and C. T. Campbell, Langmuir **16**, 9421 (2000).
[24] L. S. Jung and C. T. Campbell, J. Phys. Chem. B **104**, 11168 (2000).
[25] L. Y. Li, S. F. Chen, and S. Y. Jiang, J. Biomater. Sci., Polym. Ed. **18**, 1415 (2007).
[26] J. O. Foley, E. Fu, L. J. Gamble, and P. Yager, Langmuir **24**, 3628 (2008).
[27] M. Piliarik, H. Vaisocherova, and J. Homola, Biosens. Bioelectron. **20**, 2104 (2005).
[28] J. Homola and S. S. Yee, Sens. Actuators B **51**, 331 (1998).
[29] P. I. Nikitin *et al.*, Sens. Actuators, A **85**, 189 (2000).
[30] D. J. Oshannessy and D. J. Winzor, Anal. Biochem. **236**, 275 (1996).
[31] D. J. Oshannessy, M. Brighamburke, K. K. Soneson, P. Hensley, and I. Brooks, Anal. Biochem. **212**, 457 (1993).
[32] P. Schuck, Annu. Rev. Biophys. Biomol. Struct. **26**, 541 (1997).
[33] P. Schuck and A. P. Minton, Anal. Biochem. **240**, 262 (1996).
[34] G. S. Tamura, J. R. Hull, M. D. Oberg, and D. G. Castner, Infect. Immun. **74**, 5739 (2006).
[35] C. T. Campbell, Surf. Sci. Rep. **27**, 1 (1997).